Acoustic histology with specific dyes and antibodies

Acoustic histology with specific dyes and antibodies

Katsutoshi Miura* and Kanna Yamashita

Department of Health Science, Pathology and Anatomy, Hamamatsu University School of Medicine, Hamamatsu, Japan

*Corresponding author

Katsutoshi Miura

1-20-1 Handa-yama, Higashiku, Hamamatsu 431-3192, Japan

Tel: 81-53-435-2811

Fax: 81-53-435-2800

E-mail: kmiura@hama-med.ac.jp

Abstract

The present study aims to identify specific staining methods for acoustic histology. We compared attenuation-of-sound (AOS) images from scanning acoustic microscopy (SAM) with light microscopy (LM) images. Ethanol-fixed tissue or cytology samples and formalin-fixed surgical or autopsy specimens were examined. Nuclei, collagen, elastic fibers, and polysaccharides and various antigens, including cell surface, cytoplasmic, nuclear, and stromal substances, were observed. Samples with different fixation methods were used. Hematoxylin staining had significantly higher AOS values in accordance with staining duration. Specific staining for collagen, elastic fibers, and polysaccharides increased the AOS values of the specific substance. . Using diaminobenzidine tetrahydrochloride in $NiCl_2$ solution as a substrate for horseradish peroxidase increased the AOS values to those suitable for acoustic immunostaining. Collagenase digestion following collagen staining decreased AOS values, reflecting collagen density and distribution. Staining with specific dyes or acoustic immunostaining enabled the histological localization of specific substances by SAM, similar to LM.

Keywords: Scanning acoustic microscopy, histology, cytology, attenuation-of-sound, hematoxylin, special staining, immunostaining, collagenase

Introduction

To date, microscopic structures have been precisely examined using light microscopy (LM). Visual images of cellular and tissue components can be discriminated by staining or immunostaining using specific dyes and antibodies by LM. For acoustic images, unstained images of various tissues and cells are visualized using scanning acoustic microscopy (SAM) (Kolosov et al. 1987; Miura 2016). Whether it is possible to differentiate various tissue structures and cellular components using specific dyes and antibodies, and to assess if there are advantages in using acoustic imaging over LM remain to be elucidated.

The principles of SAM are shown in Fig. 1 (Saijo et al. 1991; Saijo 2009). Because the acoustic properties among tissues and cellular components differ, tissue and cellular imaging is possible (Brand et al. 2008; Foster et al. 2000). Saijo et al. have reported tissue characterization of gastric cancer tissues (Saijo et al. 1991) and infarcted myocardium (Saijo et al. 1997) by plotting values of attenuation coefficient (dB/mm MHz). They made hematoxylin and eosin or elastica-Masson staining slides of the neighboring sections to identify the materials within the SAM images. If a particular stain for LM imaging can also alter the acoustic properties, identification of materials

would be possible by using one SAM slide only, compared to before and after staining. Moreover, staining procedures using special dyes with specific binding capacity may be easier in SAM imaging.

In terms of the physics of ultrasound, attenuation is usually measured in units of decibels per unit length of medium (dB/mm) and is represented by the attenuation coefficient or attenuation constant of the medium (Szabo and Wu 2002). The attenuation coefficient (α) (dB/mm・MHz) can be used to determine the total attenuation in the medium using the following formula: Attenuation = α (dB/mm MHz) l(mm) f(MHz), where "l" is length and "f" is frequency. A high frequency beam is attenuated more than a lower frequency beam. Various processes influence attenuation, including reflection, refraction, scattering, and absorption. The attenuation coefficients of common biological materials at a frequency of 1 MHz are as follows (Culjat et al. 2010): water = 0.022, blood = 2.0, fat = 4.8, liver = 5.0, muscle = 10.9, connective tissue = 15.7, tendon = 47, and cortical bone = 69 (dB/mm MHz).

In general, the attenuation coefficient is low in fluid-filled structures and high in dense solid tissues. Specific dyes or materials combine particular components of cells or tissues, which produce contrast images under LM. If specific dyes and antibodies alter the local acoustic values, it is possible to detect the location of a specific

structure and function simultaneously using SAM. Here we present the successful results of staining for nuclear and extracellular components. In addition, by performing collagenase treatment post-staining, we investigate the specificity of collagen distribution.

Materials and Methods

Subjects and ethics

All human tissue sections were prepared from samples stored in tissue archives at the Hamamatsu University Hospital, Japan, or Shizuoka City Hospital, Japan. The research protocol for using stored samples without revealing patient identity was approved by the Ethics Committee of Hamamatsu University School of Medicine (No. 14-135). Written consent was waived for inclusion in this retrospective study. All methods were conducted according to approved guidelines and regulations. The cytology and tissue samples were prepared by the same methods reported previously (Miura and Yamamoto 2015) (Miura et al. 2015) as shown in Fig. 2.

SAM observations

The SAM (AMS-50AI) system used in this study was supplied by Honda Electronics

(Toyohashi, Aichi, Japan) and was equipped with a 320-MHz transducer. This resolution of the system was ~4.7 μm. The transducer was scanned on the slide to produce a two-dimensional image by plotting the AOS value of each region on the screen as shown by Saijo et al (Saijo et al. 1991; Saijo et al. 1997). Ultrasound with a pulse wave runs from a transducer and reflects off the surface of the tissue and glass slide to return to the transducer. Distilled water is used as a coupling medium. The two wave forms are separated by comparing the reference wave from the glass slide without a tissue specimen. We calculated the time and amplitude difference of the transmission through the tissue in order to obtain the values of attenuation-of-sound (AOS) through the tissue. Tissue thickness was determined using frequency characteristics of the amplitude and phase shift of reflected waves from a tissue (Okawai et al. 1990). The AOS from each point were collected and plotted on a screen.

Specific staining

Hematoxylin staining for nuclei

The cytology slides and dewaxed histology slides were soaked in commercial hematoxylin solution (Wako Pure Chemical, Osaka, Japan) for 10 min, washed

briefly in distilled water to remove excess dye and observed by SAM. The same slides were then soaked again in hematoxylin solution for 20 min or 50 min and observed in the same manner by SAM. To produce routine LM slides, eosin staining (Wako Pure Chemical, Osaka, Japan) was added after hematoxylin staining.

Feulgen reaction for DNA staining

Dewaxed slides were washed in distilled water and observed by SAM. Then, the slides were soaked in 1N HCl at 60 ˚C for 10 min and cooled in 1N HCl at 4˚C. The slides were incubated in Schiff reagent (Wako Pure Chemical, Osaka, Japan) for 30 to 60 min. Then, the Schiff reaction was stopped in 0.54% $NaHSO_3$ in 0.45N HCl solution and washed in running water. The slides were observed by SAM to compared before staining.

Aniline blue staining for collagen

The deparaffinized sections were hydrated in distilled water and soaked in 5% phosphotungstic acid solution for 10 min. The sections were then incubated in 0.4% aniline blue in 8% acetic acid solution for 10 min and rinsed twice in 1% acetic acid solution. Sections were then stored in distilled water until observation.

Sirius red staining for collagen

The dewaxed and hydrated sections were stained in picro-sirius red solution (Cosmo

Bio, Tokyo, Japan) for 1 h and washed twice in 0.5% acetic acid solution. Sections were then stored in distilled water until observation.

Weigert's resorcin-fuchsin stain for elastic fibers

The dewaxed and hydrated sections were incubated in commercial Weigert's resorcin-fuchsin solution (Merck, Darmstadt, Germany) for 1 h, washed in 100% ethanol to remove excess dye, and stored in distilled water until observation.

Oil red O, Sudan III, Sudan black B, and Nile blue for lipid staining of fresh-frozen tissues

We have used several dyes suitable for SAM of lipid staining of fresh-frozen tissues. The frozen sections were briefly washed in distilled water and soaked in 60% 2-propanol for 1 min. Slides were then incubated in Oil red O solution (Cosmo Bio, Tokyo, Japan) at 37˚C for 15 min. Overstained dyes were removed using 60% 2-propanol for 2 min and washed in running water. The slides were soaked in distilled water and observed by SAM.

For Sudan III and Sudan black B staining, the frozen sections were briefly washed in distilled water, then soaked in 50% ethanol for 30 sec. Next, the slides were incubated in either Sudan III (Merck, Osaka, Japan) at 37˚C for 60 min, or Sudan black B (Merck, Osaka, Japan) at 37˚C for 30 min. Overstained dyes were removed

by soaking in 50% ethanol for 3 min and then rinsed in running water. Slides were then soaked in distilled water and observed using SAM.

For Nile blue staining, frozen sections were briefly rinsed in distilled water and soaked in Nile blue solution (Merck, Osaka, Japan) at 60˚C for 20 min. Slides were then rinsed in distilled water for 10 sec. Overstained dyes were removed in 1% acetic acid solution for 15 min. Finally, slides were soaked in distilled water and observed using SAM.

Periodic acid-Schiff reaction

Fresh-frozen and deparaffinized sections were soaked in distilled water and oxidized in 1% periodic acid solution for 10 min. Sections were then rinsed in distilled water for 7 min and mounted with Schiff reagent (Wako Pure Chemical, Osaka, Japan) for 10 min. Finally, sections were rinsed in distilled water and observed using SAM.

Collagenase digestion

Following SAM observation, the stained slides were soaked in distilled water, and submerged into a solution of phosphate-buffered saline containing 0.5 mM $CaCl_2$ (pH 7.4) plus 250 U/mL type-III collagenase (Worthington, Lakewood, NJ, USA) at 37˚C for 1 h (Miura and Katoh 2016). According to the manufacturer's instructions, type-III collagenase has typical collagenase activity but lower proteolytic activity than

other collagenases.

Immunohistochemistry

Immunostaining was performed using a commercially available Chemmate envision kit (Dako, Glostrup, Denmark). The primary antibodies used to detect smooth muscle actin (SMA), CD20, epithelial antigen (EA) and Ki-67, respectively, were as follows: Anti-SMA (ab5694, Abcam, Tokyo, Japan; 1:400); anti-CD20 (L26, Dako, Tokyo, Japan; 1:300); anti-EA (Ber-EP4, Dako, Tokyo, Japan; 1:100), (4) anti-Ki-67 (Mib-1, Dako, Tokyo, Japan; 1:50). Heat-mediated antigen retrieval (95˚C, 20 min) was performed with buffer balanced to pH 6.0 (anti-SMA, anti-CD20, anti-Ki-67) prior to staining. Proteinase K treatment was performed for 5 min at room temperature for anti-EA antigen prior to staining.

LM observation

To compare SAM with LM images, original baseline slides were stained with HE or Elastica-Masson trichrome and with Papanicolaou stain for cytology. The same sections were then used for LM observation, or immunostaining was observed using SAM.

For immunostaining, the SAM image was compared with the LM image. The magnification of each LM image was adjusted to match the corresponding SAM image.

Statistical analyses

The average AOS values of the nuclei of hematoxylin staining were calculated from at least 10 random points per case using commercial statistics software (Statcel3-Addin forms on Excel, OMS publishing, Tokorozawa, Saitama, Japan).

Average AOS (±SD) values of baseline, 10 min post-hematoxylin stain, and 30 min or 60 min post-hematoxylin stain were compared using a Student's (unpaired) *t*-test.

Prior to conducting statistical analyses, we confirmed that each dataset followed a normal distribution using a test for the difference between averages. $P<0.05$ was considered a statistically significant difference for all tests.

Results

Hematoxylin staining for nuclei exhibited significantly increased nuclear AOS values as incubation time increased (Table 1). All of the FFPE sections (Fig. 3a), cytology (Fig. 3b) and fresh-frozen (Fig. 3c) sections exhibited significantly different AOS values of the nuclei between baseline (before staining) and 10 min incubation, and 10

181 min incubation and 30 or 60 min incubation.

182 The Feulgen reaction for DNA staining led to no apparent alteration regarding

183 SAM imaging.

184 Aniline blue staining for collagen exhibited increased AOS values at Glisson

185 capsules and septal fibrosis, accompanied by nonspecific hepatocyte staining (Fig.

186 4a). However, this nonspecific staining decreased following collagenase treatment

187 and only dense portions of collagen accumulation retained high AOS values.

188 Sirius red staining for collagen exhibited positive high AOS values in the dermal

189 collagen and the epidermis (Fig. 4b). Following collagenase treatment, the ulcer edge

190 at the left side of the figure and the surface of the epidermis retained high AOS

191 values, where dense collagen fibers and thick keratin materials escaped with

192 complete digestion. In the corresponding LM images, no remarkable staining was

193 observed.

194 Resorcin staining for elastic fibers exhibited elevated AOS values in the aortic

195 media, the values of which decreased following collagenase digestion (Fig. 4c). The

196 corresponding LM images showed no remarkable changes before versus after

197 collagenase treatment.

198 Oil red O, Nile blue, Sudan III, and Sudan black B for lipid staining of fresh-frozen

199 tissues revealed no remarkable changes on SAM imaging.

200 Following periodic acid-Schiff (PAS) staining, the AOS values of the tubular and

201 vascular basement membrane increased, which corresponded with the LM image

202 (Fig. 4d).

203 In the immunostaining of anti-SMA, the muscularis mucosae and peritubular

204 smooth muscles exhibited increased AOS values, which corresponded with the LM

205 image (Fig. 5a).

206 Anti-CD20 staining for B lymphocytes exhibited band-like infiltrate of lymphocytes

207 in the esophagus (Fig. 5b). Individual B lymphocytes also exhibited increased AOS

208 values.

209 Anti-EA stained adenocarcinoma cells in the pleural fluid of the cytology slide (Fig.

210 5c). EA antigens localized to the surface of cancer cells with high AOS values.

211 Anti-Ki67 staining showed nuclei of adenocarcinoma cells as high spotted areas,

212 corresponding to speckled positive staining in the LM image (Fig. 5d).

213

214 **Discussion**

215 The advantage of using staining in SAM measurement is being able to identify the

216 materials in acoustic images using the same unstained slides. It is possible to guess the

materials using nearby slides as a reference, by optical microscopy. However, conventional staining requires many steps and a mounting procedure prior to observation. In our current study, we omit several unnecessary steps and were able to observe slides without any mounting procedure. It is also easier and less time-consuming to identify the materials using the same unstained slide.

Hematoxylin dye combined with nuclei, and statistically increased AOS values of fresh tissues and FFPE tissues following staining were observed.

Dyes for collagen staining such as aniline blue and Sirius red raised AOS values. After collagenase digestion, these values decreased, which verified the specificity of the staining.

Resorcin dye increased the AOS values of the elastic fibers in the aorta, and these increased values declined following collagenase treatment. We observed reduced AOS values due to the fact that collagenase digested not only collagen but also other proteins like elastic fibers or coexisting smooth muscle fibers.

The PAS reaction for polysaccharides revealed higher AOS values following staining. These regions corresponded to LM-positive regions.

We have used other dyes to apply SAM to lipid and nuclear staining. Oil red O, Nile blue, Sudan III, and Sudan black B for lipid staining of fresh-frozen tissues

235 revealed no remarkable changes on SAM imaging. The Feulgen reaction for DNA
236 staining also led to no apparent alterations in SAM imaging.
237 Specific dyes available for acoustic observations have common features that
238 increase local density. First, metal components are included. Hematoxylin is oxidized
239 to form hematin, which binds with alum mordant-containing Al^{3+} ions. Positively-
240 charged Al ions combine with the negatively charged phosphate groups on DNA.
241 Another example is the immunostaining substrate Ni-DAB, which contains nickel
242 metal.
243 Second, the dyes available for acoustic staining have a high molecular weight
244 (MW) including aniline blue, molecular formula (MF): $C_{32}H_{25}N_3O_9S_3Na_2$ with a MW
245 of 732.73, Sirius red, MF: $C_{29}H_{18}N_6Na_2O_2S_2$ with a MW of 675.6, and resorcin-fuchsin
246 containing basic fuchsin, MF: $C_{20}H_{20}ClN_3$ with a MW of 337.85. Pararosanilin used
247 in the PAS reaction has a similar formula as basic fuchsin $C_{19}H_{18}ClN_3$ with a MW of
248 323.83. The above dyes combine fibrillar components consisting of repeated chemical
249 formulas.
250 In contrast, dyes found to be unsuitable for acoustic staining have a lower MW. Oil
251 Red O, MF: $C_{26}H_{24}N_4$ with a MW of 403.49, Nile blue, MF: $C_{20}H_{20}ClN_3O$ with a MW
252 of 253.85, Sudan III, MF: $C_{22}H_{16}N_4O$ with a MW of 352.39, and Sudan black B, MF:

253 $C_{29}H_{24}N_6$ with a MW of 456.54. In addition, target lipids do no exhibit repeated
254 structures such as fibers.
255 Collagenase digestion was available not only before staining but also after specific
256 staining. This procedure helped verify the specificity of the staining and also detect
257 whether the chemical modification was resistant or sensitive to digestion (Miura et
258 al. 2015; Miura and Yamashita 2018). Protein modification, including advanced
259 glycation and long oxidation of sections at room temperature, led to resistance to
260 digestion.
261 For immunostaining substrates of the HRP enzyme for SAM observation, we first
262 attempted to convert the LM method to the SAM method. DAB and peroxide are
263 regularly used as a substrate for HRP in immunostaining. However, the result in the
264 SAM observation was unsuccessful; no remarkable products appeared following
265 staining. As high density increases AOS values (Rossman et al. 1989), we used Ni-
266 DAB instead of DAB alone and succeeded in increasing the acoustic values to
267 identify antigen locations.
268 Fresh-frozen and cytology sections, in addition to the FFPE sections, were available
269 for immunostaining for SAM. Cytoplasmic, nuclear, cell surface, and stromal
270 antigens were all recognized using this method.

Several limitations of this study should, however, be acknowledged. First, the samples examined were limited by organ type, fixation methods. and the duration of fixation. We investigated various organs, including epithelial and stromal tissues, using fresh-frozen and FFPE sections, including autopsy and surgical materials, for comparison. Both specific and antibody staining were applicable to various organs with different fixation conditions. Second, staining procedures including heat treatment or pH changes may influence the outcome of acoustic properties. Sections that were not well-fixed or had an uneven surface when undergoing heating treatment became detached from the glass slides. Acidic conditions led to shrinkage producing thinner tissues, while alkaline conditions led to sections being more readily dissolved. Ethanol-fixed tissues showed this tendency although FFPE sections did not exhibit any changes. Cytology or fresh-frozen tissues must be avoided for use in these conditions.

In utilizing our current results for a future study, we plan to apply drugs or enzymes to the sections. First, anticancer drugs will be examined, including cisplatin, which is known to bind to DNA in the nucleus. If these drugs show structural changes with acoustic properties, SAM may enable the location of the drugs to be followed. Second, the function of enzymes combined to specific materials

289 in the substrate may be activated as collagenase breaks down collagens. Other
290 proteolytic or bridging reactions may be detected by changes in acoustic properties.
291 These conformational changes are difficult to follow with LM. Third, staining and
292 enzymatic reactions can be followed, according to a time course, by observing the
293 same section. Modification of inhibition or activation in the section may be possible
294 by following acoustic properties.
295 In conclusion, specific staining or immunostaining for specific tissue components
296 increased the AOS values of each corresponding component. Samples, including
297 formalin- or ethanol-fixed, or cytology sections were available for detection following
298 staining. Collagenase digestion decreased the AOS values of collagens and other
299 protein materials. Regions rich in collagen fibers were resistant to digestion,
300 retaining high AOS values than collagen-sparse areas, which reflected collagen
301 density. In immunostaining, Ni-DAB reaction products increased the AOS values,
302 indicating antigen location, using SAM. This method of acoustic staining may be
303 applicable to detect non-chromogenic substances, the detection of which is currently
304 difficult using LM imaging.
305

Acknowledgments

The authors would like to thank T. Moriki, Y. Egawa, Y. Kawabata, and N. Suzuki for preparing the histology samples. The authors would like to thank Enago (www.enago.jp) for English language review.

Funding

This work was supported by a grant from the Japan Society for the Promotion of Science (KAKENHI), Scientific Research Grant Number (c) 15K08375.

Conflicts of interest

None.

References

Brand S, Weiss EC, Lemor RM, Kolios MC. High Frequency Ultrasound Tissue Characterization and Acoustic Microscopy of Intracellular Changes. Ultrasound Med Biol 2008;34:1396-407.

Culjat MO, Goldenberg D, Tewari P, Singh RS. A review of tissue substitutes for ultrasound imaging. Ultrasound Med. Biol. 2010;36:861-73.

Foster FS, Pavlin CJ, Harasiewicz KA, Christopher DA, Turnbull DH. Advances in ultrasound biomicroscopy. Ultrasound Med. Biol. 2000;25:1-27.

Kolosov O V, Levin VM, Mayev RG, Senjushkina TA. The use of acoustic microscopy for biological tissue characterization. Ultrasound Med Biol Pergamon Press. 1987;13:477-83.

Miura K. Application of Scanning Acoustic Microscopy to Pathological Diagnosis. Microsc Anal 2016.

Miura K, Egawa Y, Moriki T, Mineta H, Harada H, Baba S, Yamamoto S. Microscopic observation of chemical modification in sections using scanning acoustic microscopy. Pathol Int 2015;65:355-66.

Miura K, Katoh H. Structural and Histochemical Alterations in the Aortic Valves of Elderly Patients: A Comparative Study of Aortic Stenosis, Aortic Regurgitation, and Normal

337 Valves. Biomed Res Int 2016;2016.

338 Miura K, Yamamoto S. A scanning acoustic microscope discriminates cancer cells in fluid.

339 Sci Rep 2015;5:15243.

340 Miura K, Yamashita K. Evaluation of aging, diabetes mellitus, and skin wounds by

341 scanning acoustic microscopy with protease digestion. Pathobiol Aging Age-related Dis

342 2018;8:1516072.

343 Okawai H, Tanaka M, Dunn F. Non-contact acoustic method for the simultaneous

344 measurement of thickness and acoustic properties of biological tissues. Ultrasonics

345 1990; 28:401-10.

346 Rossman P, Zagzebski J, Mesina C, Sorenson J, Mazess R. Comparison of speed of sound

347 and ultrasound attenuation in the os calcis to bone density of the radius, femur and

348 lumbar spine. Clin Phys Physiol Meas 1989;10:353.

349 Saijo Y. Acoustic microscopy: latest developments and applications. Imaging Med London:

350 2009;1:47-63.

351 Saijo Y, Tanaka M, Okawai H, Dunn F. The ultrasonic properties of gastric cancer tissues

352 obtained with a scanning acoustic microscope system. Ultrasound Med Biol Pergamon

353 Press 1991;17:709-14.

354 Saijo Y, Tanaka M, Okawai H, Sasaki H, Nitta S-I, Dunn F. Ultrasonic tissue

characterization of infarcted myocardium by scanning acoustic microscopy. Ultrasound Med Biol Pergamon Press 1997;23:77-85.

Szabo TL, Wu J. A model for longitudinal and shear wave propagation in viscoelastic media. J Acoust Soc Am 2002;107:2437-46.

362 **Figure legends**

363 Fig. 1. Principles of SAM

364 In SAM, the AOS values are plotted on a screen to produce images. The AOS values

365 usually increase with density. SAM, scanning acoustic microscopy; AOS, attenuation-

366 of-sound.

367

368 Fig. 2. Flow chart of sample preparation

369 SAM, scanning acoustic microscopy

370

371 Fig. 3. Changes in AOS values following hematoxylin staining

372 a: Gastric carcinoma on formalin-fixed and paraffin-embedded section. The graphs

373 show average±SD of AOS. AOS values significantly increased ($p < 0.01$), according to

374 the length of incubation in hematoxylin dye, between 0 min (baseline) to 10 min and

375 10 min to 60 min. The representative areas are circled on the figure. The right upper

376 image is the corresponding LM images after 60 min incubation in hematoxylin.

377 b: Cytology of adenocarcinoma (lung primary) in ascites. Ethanol-fixed carcinoma cells

378 exhibited a gradual increase in AOS values from 0 min (baseline) to 10 min and 60

379 min after hematoxylin incubation (circle). The graphs show average ± SD of AOS. AOS

380 values were significantly different ($p<0.001$) from 0 min (baseline) to 10 min, and 10
381 min to 60 min. The right upper image is the corresponding LM images after 60 min
382 incubation in hematoxylin.
383 c: Glioblastoma of the brain, fresh-frozen section. Nuclei of the glioblastoma cells in
384 dotted images show progressively increased AOS values following staining. The
385 graphs show average ± SD of AOS. AOS values significantly increased ($p < 0.01$) from
386 0 min (baseline) to 10 min, and 10 min to 30 min. The representative areas were
387 circled on the figure. The right upper image is the corresponding LM images after 30
388 min incubation in hematoxylin.
389 AOS, attenuation-of-sound; LM, light microscopy; Circles, regions of interest for
390 comparison
391
392 Fig. 4
393 Changes in AOS values following specific staining
394 a: Aniline blue staining of liver cirrhosis section and its post-collagenase digestion.
395 Unstained baseline images were altered to accentuate the fibrous portion following
396 staining, while accentuated images decreased following collagenase treatment. The
397 representative areas were circled on the figure. The corresponding LM images are

shown on the lower row.

b: Sirius red stain for collagen fibers of skin ulcer section. Unstained baseline image displayed a higher portion at the left side of the dermis (circle), which is coincident with fibrous ulcer bed. The baseline image changed to emphasize collagen fibers in the dermis, which values decreased following collagenase treatment. The corresponding LM images are displayed on the lower row.

c: Resorcin-fuchsin stain for elastic aortic fibers

Aortic media with increased AOS values following staining, which decreased slightly following collagenase digestion (circle). The intima and externa exhibited no remarkable changes. The corresponding LM images are displayed on the lower row. The LM image following collagenase showed no remarkable changes.

d: PAS reaction for polysaccharides in kidney section.

Glomerular and tubular basement membrane (circle) showed greater AOS values following PAS staining. The corresponding LM images in hematoxylin-eosin and PAS staining are displayed on the lower row. AOS, attenuation-of-sound; LM, light microscopy; PAS, Periodic acid-Schiff.

Fig. 5

Immunostaining using 3,3'-diaminobenzidine tetrahydrochloride (DAB) in $NiCl_2$ solution as a substrate for horseradish peroxidase

a: Gastric mucosa stained with anti-smooth muscle actin (SMA). Muscularis mucosae and peri-glandular smooth muscles (circle) exhibited high attenuation portions following staining. The corresponding hematoxylin-eosin and LM images following immunostaining are shown on the lower row.

b: Esophagus with lymphocytic infiltration. Lymphocytes in the wall of the esophagus exhibited high AOS values following immunostaining with anti-CD20 (circle). The corresponding hematoxylin-eosin image and LM image following immunostaining are shown on the lower row.

c: Adenocarcinoma in pleural effusion (cytology). Adenocarcinoma cells with irregular contour exhibited high AOS values following staining with anti-epithelial (EA) antigen at the surface (circle). Background small lymphocytes were negative. The corresponding Papanicolaou staining image and LM immunostaining images are shown on the lower row.

d: Adenocarcinoma cells in ascites (cytology). Immunostaining with anti-Ki-67. Adenocarcinoma cells forming clusters showed dotted high AOS regions in the cluster, which corresponded to cancer cell nuclei (circle). The corresponding Papanicolaou

staining image and LM immunostaining images are shown on the lower row. AOS, attenuation-of-sound; LM, light microscopy.

Table 1. Average attenuation of sound (AOS) post-hematoxylin staining

	Data n	Average AOS dB/mm	SD	
Gastric ADC(histology)				
Baseline	10	5.12	0.67	**
Hemato10 min	10	7.35	1.13	
Hemato60 min	10	8.61	0.67	**
Lung ADC(cytology)				
Baseline	15	4.72	0.30	***
Hemato10 min	15	5.95	0.50	
Hemato60 min	15	7.55	0.83	***
GB(Frozen section)				
Baseline	5	4.42	0.79	**
Hemato10 min	5	8.34	1.74	
Hemato30 min	5	13.16	2.53	**

ADC; adenocarcinoma, Baseline; before staining, HematoXmin; incubation in hematoxylin for X min, GB; glioblastoma

**p < 0.01, ***p < 0.001

Fig. 1

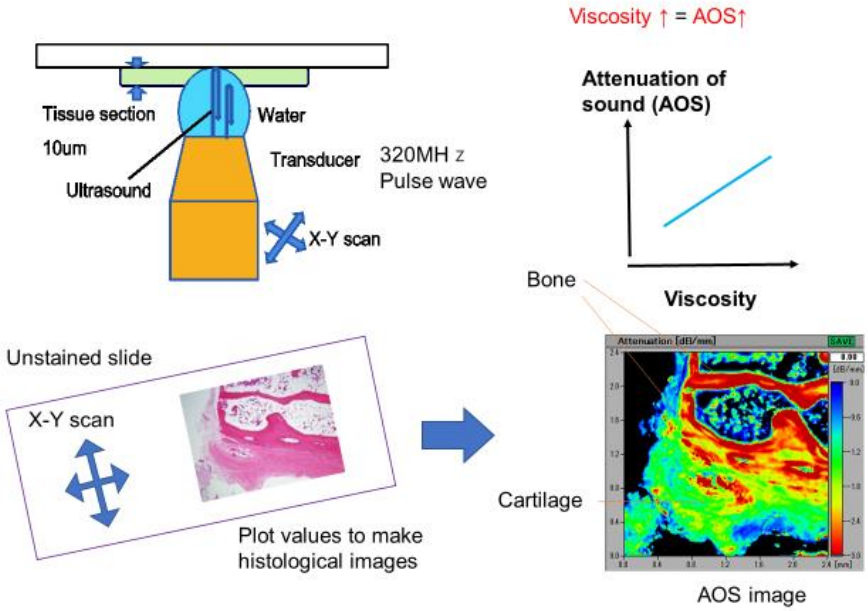
Tissue section
10um
Water
Ultrasound
Transducer
320MH z
Pulse wave
X-Y scan
Unstained slide
X-Y scan
Plot values to make
histological images
Viscosity ↑ = AOS↑
Attenuation of
sound (AOS)
Bone
Viscosity
Cartilage
AOS image

Fig. 2

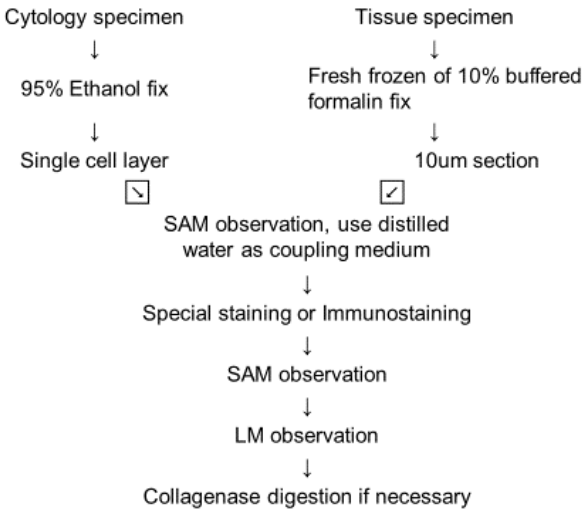
Cytology specimen
Tissue specimen
95% Ethanol fix
Fresh frozen of 10% buffered formalin fix
Single cell layer
10um section
SAM observation, use distilled water as coupling medium
Special staining or Immunostaining
SAM observation
LM observation
Collagenase digestion if necessary

Fig. 3a

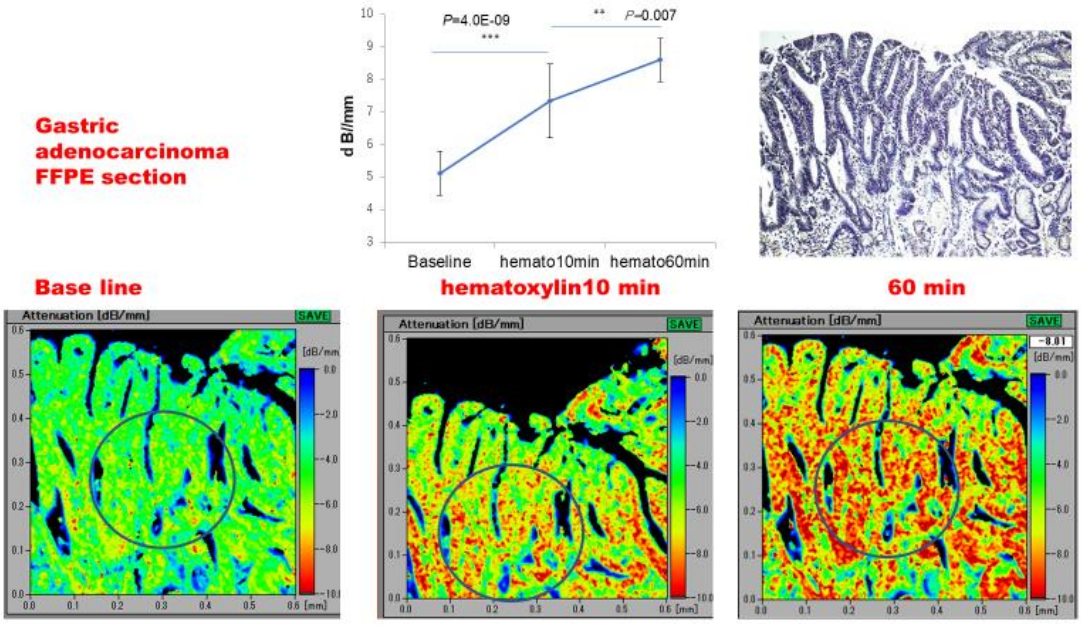
Gastric
adenocarcinoma
FFPE section
P=4.0E-09
***
**
P=0.007
dB/mm
Baseline
hemato10min
hemato60min
Base line
hematoxylin10 min
60 min
Attenuation [dB/mm]
SAVE

Fig. 3b

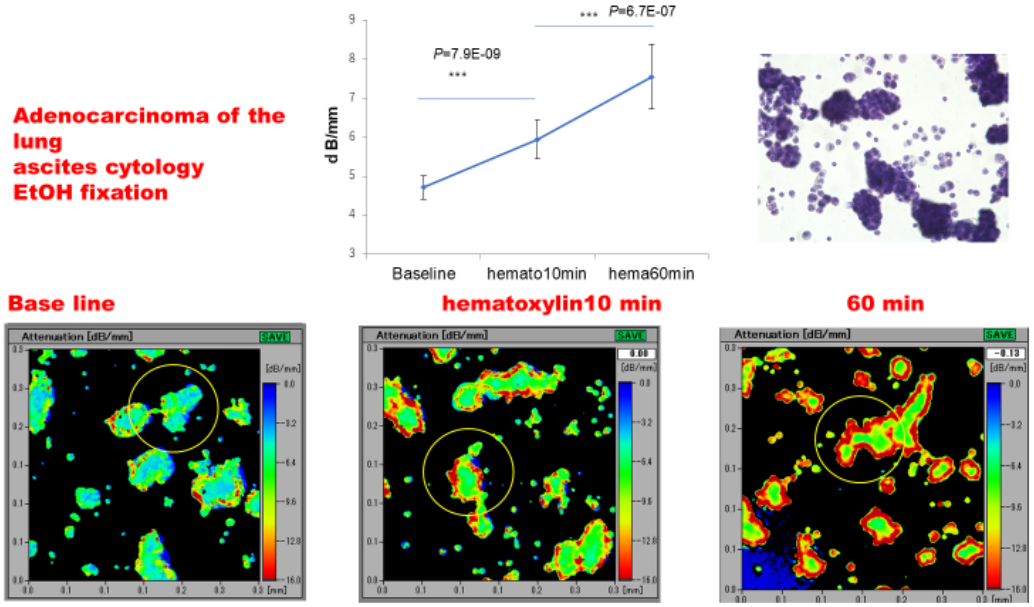
Adenocarcinoma of the lung
ascites cytology
EtOH fixation
*** P=6.7E-07
P=7.9E-09
***
dB/mm
Baseline
hemato10min
hema60min
Base line
hematoxylin10 min
60 min
Attenuation [dB/mm]
SAVE

Fig. 3c

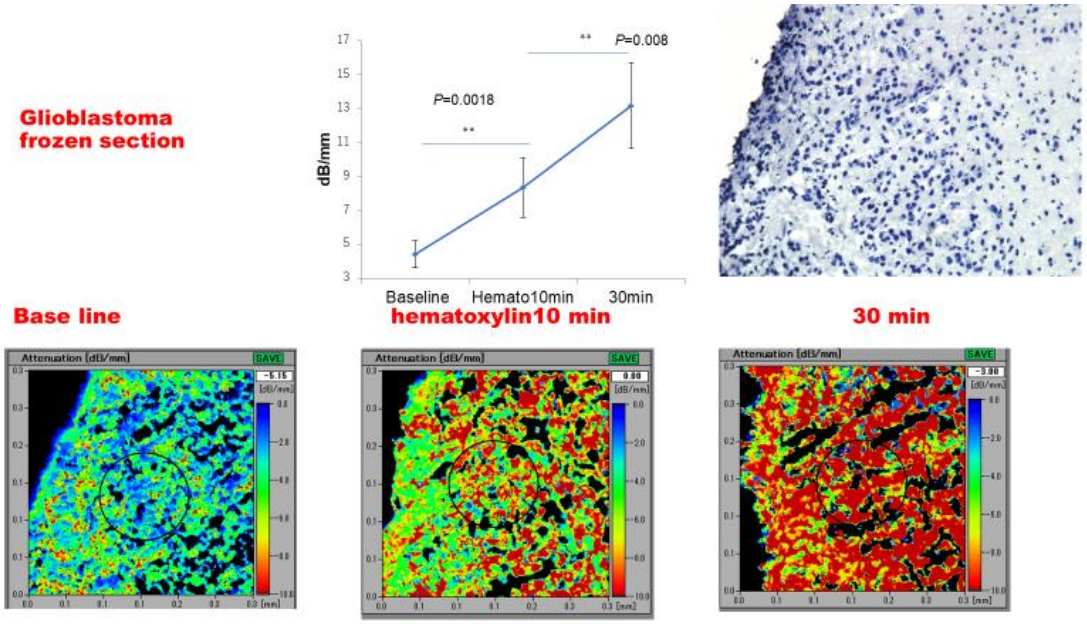
Glioblastoma
frozen section
dB/mm
17
15
13
11
9
7
5
3
P=0.0018
**
**
P=0.008
Baseline
Hemato10min
30min
Base line
hematoxylin10 min
30 min
Attenuation [dB/mm]
SAVE

Fig. 4a

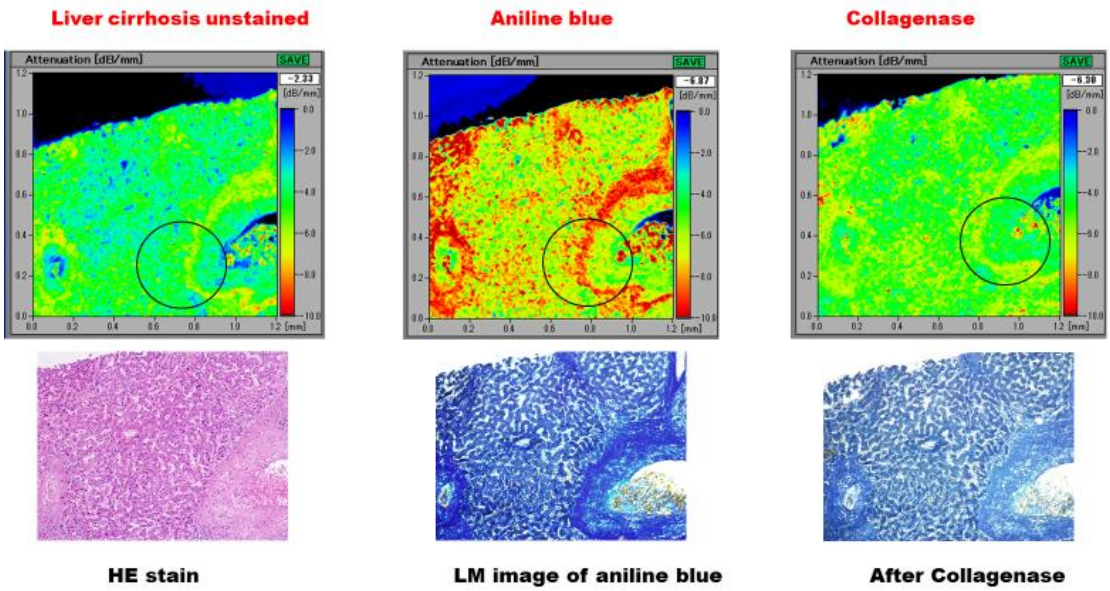
Liver cirrhosis unstained
Aniline blue
Collagenase
Attenuation [dB/mm]
SAVE
HE stain
LM image of aniline blue
After Collagenase

Fig. 4b

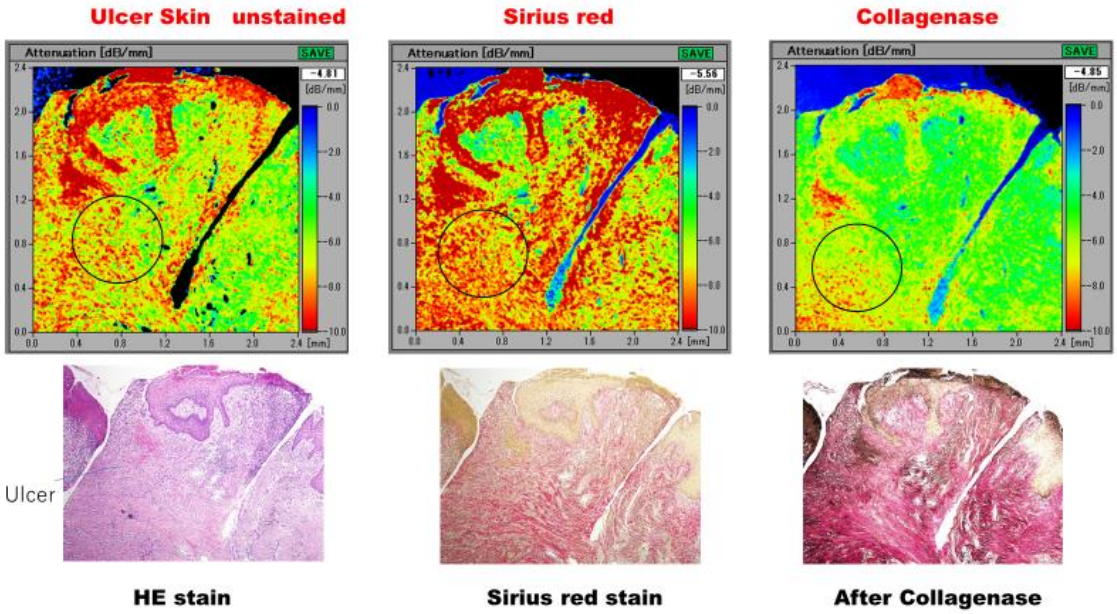
Ulcer Skin unstained
Sirius red
Collagenase
Attenuation [dB/mm]
SAVE
Ulcer
HE stain
Sirius red stain
After Collagenase

Fig. 4c

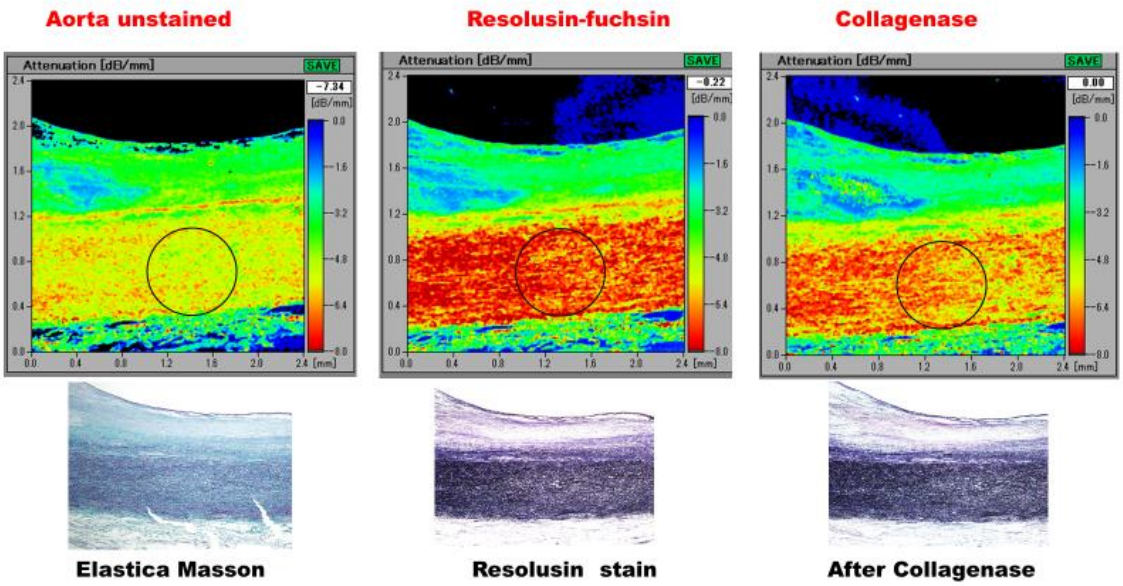
Aorta unstained
Resolusin-fuchsin
Collagenase
Attenuation [dB/mm]
SAVE
Elastica Masson
Resolusin stain
After Collagenase

Fig. 4d

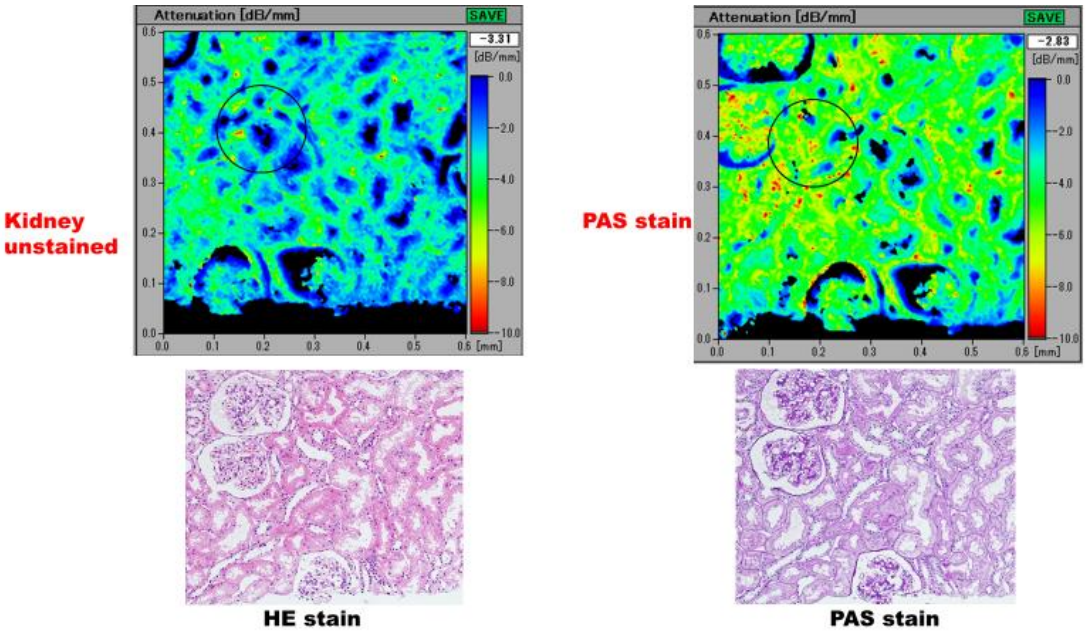
Kidney unstained
Attenuation [dB/mm]
SAVE
−3.31
[dB/mm]
[mm]
PAS stain
Attenuation [dB/mm]
SAVE
−2.83
[dB/mm]
[mm]
HE stain
PAS stain

Fig. 5a

Gastric adenocarcinoma unstained

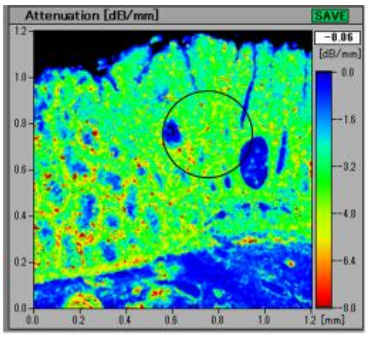

Anti-SMA

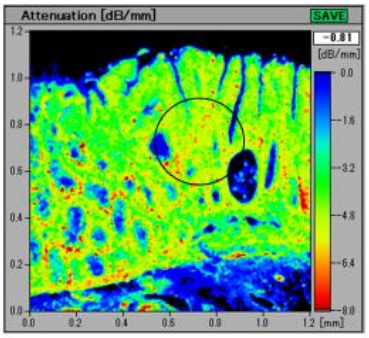

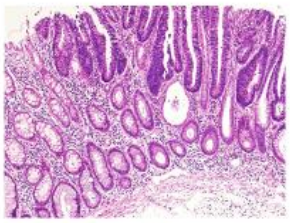

HE stain

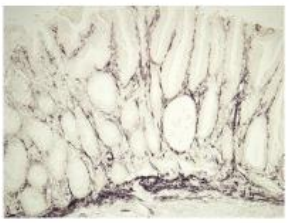

LM image of anti-SMA stain

Fig. 5b

Esophagus carcinoma in situ unstained

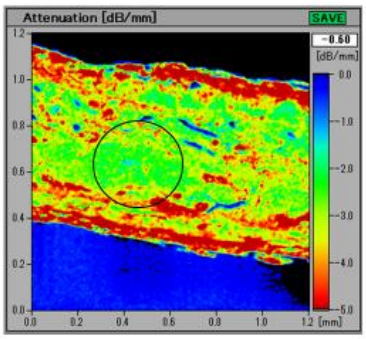

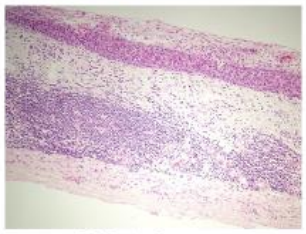

HE stain

Anti-CD20

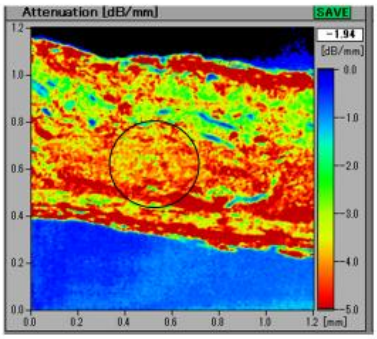

LM image of anti-CD20 stain

Fig. 5c

Adenocarcinoma in pleural effusion (cytology) unstained

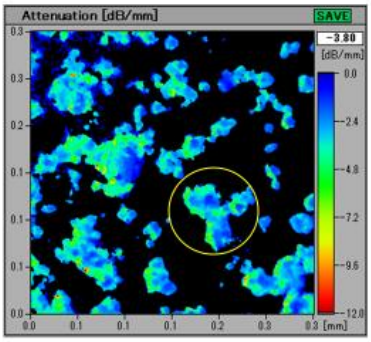

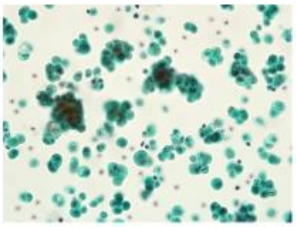

Papanicolaou staining

Anti-AE

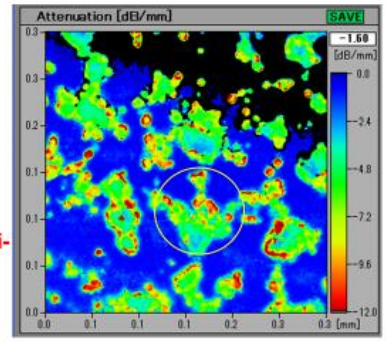

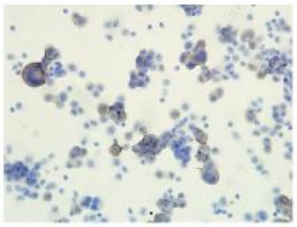

LM image of anti-CD20 stain

Fig. 5d

Adenocarcinoma in ascites (Cytology) unstained

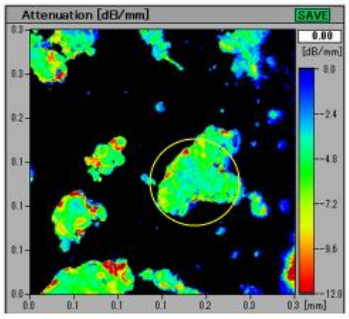

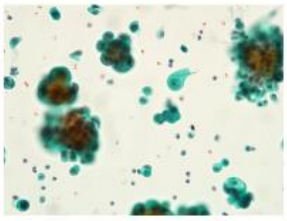

Papanicolaou staining

Anti-Ki 67

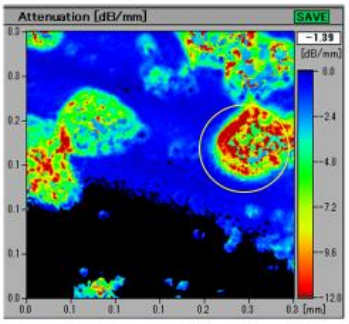

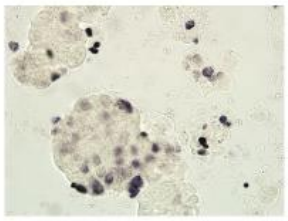

LM image of anti-Ki 67 stain